Heme–CO Religation in Photolyzed Hemoglobin: A Time-Resolved Raman Study of the Fe–CO Stretching Mode†

M. C. Schneebeck,‡ L. E. Vigil,‡ J. M. Friedman,§ M. D. Chavez,*,‡,∥ and M. R. Ondrias*,‡

Department of Chemistry, University of New Mexico, Albuquerque, New Mexico 87131, and Department of Physiology and Biophysics, Albert Einstein College of Medicine, Bronx, New York 10461

Received June 10, 1992; Revised Manuscript Received November 10, 1992

ABSTRACT: Time-resolved resonance Raman spectroscopy has been employed to monitor geminate heme–CO rebinding in photolyzed HbCO. The excitation frequency was tuned to enhance the scattering from rebound heme sites 20–500 ns subsequent to CO photolysis. The behavior of ν_{Fe-C} during ligand rebinding has important ramifications concerning heme pocket dynamics of the distinct equilibrium configurations of the six-coordinate heme sites. During the geminate phase of recombination, the Fe–CO bond strengths and configurations of the rebound sites (inferred from the positions and line widths of ν_{Fe-C}) were found to be the same as those of equilibrium configurations of HbCO within 500 ns of CO photolysis for all samples. No evidence was found for the existence of transient metastable configurations during geminate recombination. Spectra obtained at earlier times (100 ns) revealed small differences in the geminate rebinding rates of the two equilibrium configurations. Since there is little or no further CO rebinding between 100 and 500 ns after photolysis, some interconversion must occur between the dominant HbCO configurations on a submicrosecond time scale.

During the past decade, it has become increasingly evident that dynamics play an important role in determining the reactivity of heme proteins (Debrunner & Frauenfelder, 1982; Karplus & McCammon, 1983). The complexity of the multilevel dynamics of proteins makes it highly desirable to examine systems where both the kinetic rates and the equilibrium structures are very well characterized. Thus, the mechanism of ligand binding of hemoglobins and myoglobins provides a nearly ideal framework in which to explore the roles of structural dynamics in the functions of heme proteins.

The specificity and interpretability of resonance Raman scattering from hemes make it an excellent technique for time-resolved structural characterizations of the active sites of hemoglobin (Rousseau & Friedman, 1988; Spiro, 1983; Rousseau & Ondrias, 1983; Friedman et al., 1982a). In particular, the resonance Raman spectra of photolytic hemoglobin transients have been well characterized (Rousseau & Friedman, 1988; Scott & Friedman, 1984; Findsen et al., 1985a,b, 1986, 1988; Stein et al., 1982; Terner et al., 1981; Dasgupta et al., 1985; Friedman et al., 1982b; Ondrias et al., 1983; Friedman, 1984; Carson et al., 1987). Although several heme normal modes display time-dependent behavior, the axial ligand modes are the most useful for inferring the heme pocket dynamics associated with ligand binding. The mode identified with stretching motion of the heme Fe and the proximal histidine [see Rousseau and Friedman (1988)] is particularly informative concerning the dynamics of photolyzed deoxy hemes. The behaviors of the Fe–C and C–O stretching modes similarly are useful for determining the heme–ligand interactions of HbCO. These modes have been extensively characterized in equilibrium hemoglobins under a variety of conditions [Kerr & Yu, 1988; Li and Spiro (1988) and references therein].

To date, time-resolved resonance Raman spectroscopy has been used to characterize only the deoxy transient species produced by ligand photolysis from hemoglobins. We have extended these studies to include transient six-coordinate species (i.e., religated hemes) contained within protein structures that have undergone varying degrees of relaxation toward the T-state configuration. By examining the time-dependent behavior of the Fe–C stretching mode, the structural evolution of heme sites that have rapidly (<500 ns) rebound CO subsequent to photolysis can be analyzed.

MATERIALS AND METHODS

Human hemoglobin (Hb) was purified from fresh, whole cells following a modification of the procedure of Antonini and Brunori (1971). Samples were prepared for resonance Raman spectroscopy as follows: Stock (~5.5 mM) solutions of Hb were placed in anaerobic cuvettes, diluted to ~200 μM in appropriate buffered solutions, and partially deoxygenated by several pump/purge cycles with N_2 gas, followed by the addition of a slight excess of sodium dithionite. These samples were then placed under 1 atm of CO_2-free ^{12}CO or ^{13}CO.

Samples were prepared for infrared spectroscopy by dialysis of the stock solutions (Spectrapor 6000–8000 MW cutoff) for 6 h in appropriate buffer systems (0.1 M citric acid for pH 4.5, 0.1 M Bis-Tris and ~40 mM inositol hexaphosphate for pH 6.5 + IHP). The dialysis buffer was changed frequently and vigorously bubbled with CO prior to removal of the dialyzed HbCO sample. After dialysis, the concentration of HbCO was determined to be 4.5 mM. The pH values of the sample solutions were checked after the spectroscopic studies and did not change.

Nanosecond time-resolved resonance Raman spectra of rebound heme sites were obtained via protocols previously used to investigate deoxy Hb phototransients (Scott & Friedman, 1984; Findsen et al., 1988). In this case, however,

† This work was performed at the University of New Mexico and supported by the NSF (DMB8604435) and the NIH (RR08139 and GM 33330). M.C.S. is a Howard Hughes predoctoral fellow.

* To whom correspondence should be addressed.

‡ University of New Mexico.

§ Albert Einstein College of Medicine.

∥ Present address: Laboratory of Biophysical Chemistry, National Heart, Lung, and Blood Institute, National Institutes of Health, Bethesda, MD 20892.

0006-2960/93/0432-1318$04.00/0

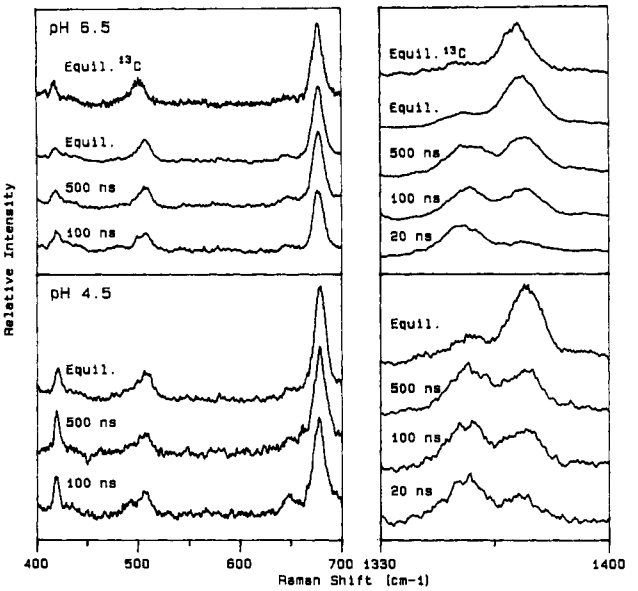

FIGURE 1: Time-resolved resonance Raman spectra of photolyzed HbCO during geminate recombination. Upper panels: pH 6.5 + IHP. Lower panels: pH 4.5. Times listed above spectra denote the Δt between 532-nm pump pulses and 413-nm probe pulses. Spectra of equilibrium species were obtained by using a probe-only protocol. The uppermost spectrum of the pH 6.5 data shows the effects of ^{13}CO isotopic substitution. Data are the unsmoothed sums of 3–6 scans at 15 cm^{-1}/min with a spectral band pass of 5–7 cm^{-1} (see text for additional details).

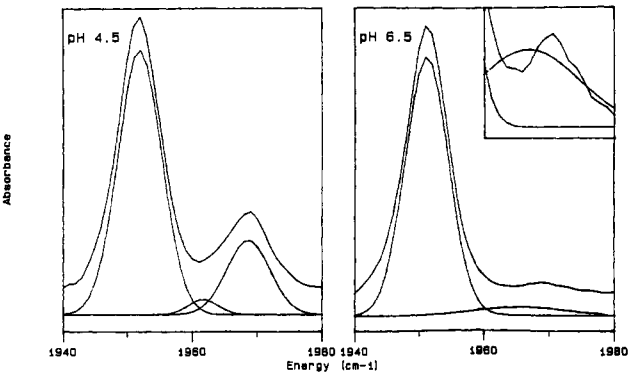

FIGURE 2: FTIR spectra of equilibrium HbCO at pH 4.5 (left) and pH 6.5 + IHP (right). The upper trace in each panel represents the experimental data. The bands corresponding to the "best-fit" deconvolution are displayed below each spectrum for clarity. The inset shows the inadequacy of the fit to the minor band at pH 6.5 + IHP. The spectra are the average of 256 scans. A background spectrum for each buffer condition was subtracted from the appropriate sample spectrum (see text for details).

the probe laser wavelength was tuned to maximally enhance resonance Raman scattering from CO-bound hemes (i.e., those hemes that had rebound the photolyzed ligand in the Δt between pump and probe pulses). Probe laser flux was attenuated with neutral density filters and focusing optics until it produced minimal CO photolysis (1×10^8 W/cm^2; 10 Hz) (see Figure 1). The pump laser intensity was adjusted to ensure maximal photodissociation of the sample ($>1 \times 10^9$ W/cm^2; 10 Hz). The degree of photolysis was monitored by scanning the region 1330–1400 cm^{-1}, where HbCO and deoxy Hb exhibit well-separated peaks at 1373 and 1357 cm^{-1}, respectively. Spectra were obtained at Δt values ranging from 20 ns to 5 μs, with an uncertainty of $\pm$10 ns due to electronic limitations. Sapphire windows were used in the sample cells to avoid the broad scattering exhibited by quartz in the 450–500-cm^{-1} region. The sharp line at 420 cm^{-1} in the spectra arises from sapphire and was used to verify instrument calibration. Samples were monitored with UV/vis spectroscopy before and after the resonance Raman measurements to ascertain that no sample degradation had occurred.

Infrared spectra were obtained by using a Perkin-Elmer Model 1600 Fourier transform spectrometer. Samples were placed in cells having an IR-tran back window and a Cleartran front window (Buck Sciencific) separated by a 0.05-mm spacer. Background spectra were obtained for each buffer.

Spectra were deconvoluted and analyzed as follows. The baseline was adjusted by using a two-point linear correction. Both the resonance Raman and FTIR spectra were then deconvoluted into two or three Gaussian bands that were allowed to vary in line width, position, and intensity in order to minimize χ^2 values. For the pH 6.5 + IHP FTIR data, the initial parameters were two Gaussians, each with full width at half-maximum of 8.0 cm^{-1}, one at 1951 cm^{-1} and the other at 1968 cm^{-1}. Reasonable convergence was reached in less than 20 iterations. The adequacy of the fits was evaluated by subtracting the simulated curves from the real spectra. Fits were limited to components comprising >2% of the integrated intensity. A similar procedure was used to analyze the time-resolved RRS data by using the Gaussian bands of fwhm = 15 cm^{-1} positioned at ~490 and ~505 cm^{-1} as initial approximations. The lower signal-to-noise ratios of the RRS spectra clearly limit the quantitative utility of the simulated spectra in these cases.

RESULTS

Figures 1 and 2 depict resonance Raman spectra in the 400–700- and 1330–1400-cm^{-1} regions and FTIR spectra in the C–O stretching region obtained from equilibrium HbCO at pH 6.5 in the presence of IHP and at pH 4.5 (no IHP). Lowering the pH from 6.5 to 4.5 significantly increases the heme–ligand configurational heterogeneity in equilibrium HbCO. This is apparent in the pH-dependent behavior of equilibrium $\nu_{C=O}$ and ν_{Fe-C}.

FTIR absorption studies of the $\nu_{C=O}$ vibrational frequency reveal multiple, discrete structural states of the equilibrium CO–heme–protein complex whose relative populations are pH sensitive. Under conditions of pH 6.5 + IHP, two peaks are obvious in the spectrum (Figure 2): a major, symmetric band at 1951 cm^{-1} and a minor band at 1969 cm^{-1}. When the HbCO is exposed to pH 4.5, a shift in the relative intensities of these two bands is seen, and the presence of a third peak becomes apparent. The major band appears relatively unchanged in shape and position at 1952 cm^{-1}. The minor band has grown in intensity and is clearly asymmetric, with a maximum at 1969 cm^{-1}. The asymmetry of this minor peak suggests that more than one structural form contributes to it.

These data were further analyzed by Gaussian deconvolution, the results of which are presented in Figure 2 and summarized in Table I. The FTIR spectra were adequately described by two and three Gaussian bands for the pH 6.5 + IHP and pH 4.5 data, respectively. Under conditions of pH 6.5 + IHP, spectral analysis yields a large Gaussian peak with a maximum at 1951 cm^{-1} and a much smaller Gaussian with a maximum at 1966 cm^{-1}. Closer inspection of the Gaussian fit to the small peak (see inset, Figure 2) shows that the fit curve does not coincide well with that of the original data. By analogy to the pH 4.5 data (see below), there is probably a third, extremely weak peak under the absorption envelope, but its intensity is below the reliable dynamic range of the curve-fitting program. At pH 4.5, the presence of a third peak is required to achieve a good fit. The major band appears at 1952 cm^{-1} and now comprises significantly less of the total

Table I[a]

	Δt	ν_{FeC} (cm^{-1})	Γ (cm^{-1})	% area	ν_{C-O} (cm^{-1})	Γ (cm^{-1})
pH 6.5 + IHP	equil	487 ± 5	17 ± 2	16 ± 3	1969 ± 2	7 ± 2
		507 ± 1	16 ± 2	84 ± 3	1951 ± 1	93 ± 2
	equil	484 ± 5	13 ± 2	15 ± 3		
	^{13}CO	502 ± 1	16 ± 2	85 ± 3		
	100 ns	480 ± 5	17 ± 2	21 ± 3		
		506 ± 1	17 ± 2	79 ± 3		
	500 ns	487 ± 5	17 ± 2	15 ± 3		
		507 ± 1	16 ± 2	85 ± 3		
HbA, pH 4.5	equil	493 ± 5	17 ± 2	29 ± 3	1969/1962 ± 2	22 ± 2
		509 ± 1	15 ± 2	71 ± 3	1952 ± 1	78 ± 2
	100 ns	492 ± 5	15 ± 2	41 ± 3		
		508 ± 1	13 ± 2	59 ± 3		
	500 ns	493 ± 5	13 ± 2	28 ± 3		
		507 ± 1	13 ± 2	72 ± 3		

[a] All peak positions, line widths, and areas are obtained from curve fits described in the text.

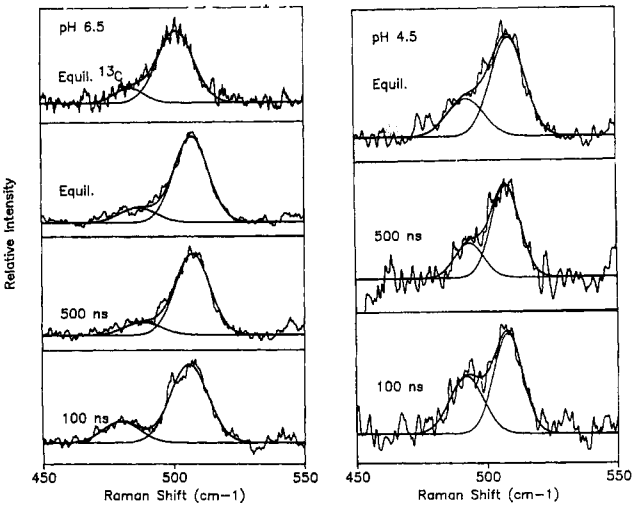

FIGURE 3: Deconvolutions of the ν_{Fe-C} regions of the data in Figure 1. The bands corresponding to the "best-fit" deconvolution are superimposed on the raw data. The times listed above spectra denote Δt between 532-nm pump and 406-nm probe pulses. Equilibrium spectra were obtained by using a probe-only protocol (see text for details).

integrated intensity. The broad, low-intensity band seen in the pH 6.5 + IHP data is now much more intense than at the higher pH and is composed of two bands (1969 and 1962 cm^{-1}). The bandwidths of all three peaks are similar and reasonable for IR absorption by a single species [see Li and Spiro (1988)]. Analogous pH-dependent behavior is observed for ν_{Fe-C} in the equilibrium resonance Raman spectra. Although only two bands are resolved under both pH 4.5 and pH 6.5 + IHP conditions, the relative intensity of the minor band at ~490 cm^{-1} increases when the pH is lowered. These data and their deconvolutions are presented in Figure 3 and summarized in Table I.

Time-resolved resonance Raman spectra obtained from photolyzed HbCO samples over the first 500 ns subsequent to photodissociation provide a means of establishing both the extent to which geminate recombination occurs via transient distal pocket structures and the influence of the relaxing proximal heme pocket on the structure of the reformed heme–ligand pair (Figure 1). The behavior of ν_4 (1373 cm^{-1} for HbCO; 1357 cm^{-1} for unligated Hb) clearly shows that the probe pulses (413 nm) alone do not significantly photolyze the sample. Religation is apparent in the growth of the 1373-cm^{-1} peak subsequent to photolysis. The small amount of intensity at 1373 cm^{-1}, occurring in the Δt = 20 ns spectra, can be attributed to fast geminate recombination (Friedman & Lyons, 1980). This is not unexpected since the probe pulse is tuned to maximize Raman intensity for the ligated heme sites. The Fe–CO stretching mode (at ~507 cm^{-1}) of the rebound heme sites was monitored during the geminate recombination phase of the ligand binding dynamics. The much weaker Fe–C–O bending mode (~570 cm^{-1}) was not apparent at the signal-to-noise ratio of the transient spectra. Within 100 ns of photolysis, enough geminate recombination had occurred to obtain a reproducible spectrum of the ν_{Fe-C} region. Differences in the relative intensities of the two ν_{Fe-C} bands (relative to equilibrium HbCO) are apparent on this time scale. In contrast, no significant changes in either the position or line shape of the major ν_{Fe-C} band at 507 cm^{-1} were observed between equilibrium HbCO and the rebound sites on a 500-ns time scale. The time-dependent behavior of ν_{Fe-C} was qualitatively similar at both pH values.

Figure 3 and Table I summarize the results of deconvoluting the time-resolved RRS data for samples at pH 6.5 + IHP and pH 4.5. In all cases, reasonable fits required a weak mode at ~480–495 cm^{-1} and a strong band at 505–510 cm^{-1} (see Table I). The weak band is assigned as a second ν_{Fe-C} on the basis of its sensitivity to ^{13}CO isotopic substitution. Clearly, the spectra obtained at Δt = 500 ns are equivalent to the spectra of analogous equilibrium HbCO samples. At earlier times, however, small but reproducible differences are apparent in the relative intensities (but not line shapes) of the ~490- and ~510-cm^{-1} bands between the rebound and equilibrium heme sites, particularly for the pH 4.5 sample.

DISCUSSION

During the past 10–15 years, it has been convincingly demonstrated that the binding of small ligands to Hb and Mb is not a simple process. Spectroscopic studies (most notably those of Frauenfelder and co-workers) have characterized the nonexponential rebinding kinetics over an extended range of time, temperature, and solution conditions. The complexity of this process is predicted in large measure on (1) structural heterogeneity at the equilibrium heme active sites and (2) structural dynamics occurring within the heme pocket during the ligand binding process. Analysis of the Fe–C and C–O stretching modes provides an excellent probe for structural changes occurring at the heme site. Thus, the time-resolved data obtained in this study directly address CO rebinding rates and the structural evolution of the six-coordinate heme–CO immediately subsequent to CO rebinding in photolyzed HbCO.

Heterogeneity at the Active Site of Hemoglobin and Myoglobin. Structural heterogeneity at the active sites of MbCO and HbCO is apparent on two distinct levels. Different equilibrium heme–ligand geometries are possible and manifest themselves as discrete ν_{Fe-C} and $\nu_{C=O}$ bands in the resonance Raman and IR spectra, respectively, of the equilibrium species. Further conformational variability within these configurations results in the inhomogeneous broadening of the distinct Fe–C and C–O bands.

The configurational heterogeneity of MbCO has been extensively characterized. Sperm whale myoglobin has at least two distinct C–O bands (1946 and 1966 cm^{-1}) at room temperature (Ansari et al., 1987; Chance et al., 1987; Makinen et al., 1979; Shimada & Caughey, 1982; Morikis et al., 1989) that correspond to distinct Fe–C bands (508 and 491 cm^{-1}, respectively). The MbCO spectra are qualitatively similar to those observed for HbCO in that a major band dominates the spectrum, a minor band appears at higher frequency, and the relative intensities of these bands are pH-dependent. However, deconvolution of the Mb–CO spectra yields four, rather than the two or three, distinct components seen in HbCO (see below). Unfortunately, at room temperature, MbCO exhibits a very low geminate yield (Friedman & Lyons, 1980; Hofrichter et al., 1983). Thus, the population of rebound active sites is too small to be detected accurately at $\Delta t < 10$ μs by using time-resolved resonance Raman techniques. Hb, on the other hand, exhibits significant submicrosecond geminate heme–CO recombination, thereby lending itself to time-resolved resonance Raman investigation.

While the dominant configuration in HbCO ($\nu_{C=O}$ at $\sim$1951 cm^{-1} and ν_{Fe-C} at $\sim$507 cm^{-1}) accounts for the large majority of the population, structural heterogeneity is apparent in the Hb heme pocket, especially at low pH. Under pH 7.4 conditions, Potter et al. (1990), found four different C=O components in the IR spectra of HbCO. Decreasing the pH leads to an increase in the intensity of the peak at about 1969 cm^{-1} and a concomitant decrease in the intensity of the major peak at 1951 cm^{-1} (Potter et al., 1990). Deconvolution of our spectra obtained at pH 4.5 shows only three component peaks. The larger shift in relative integrated intensity between the 1952- and 1969-cm^{-1} peaks seen in this laboratory most likely results from different experimental conditions between the two studies. However, it is clear that the major components of our HbCO spectra and the general behavior observed in response to changes in pH are consistent with those observed by Potter et al.

Deconvolution of the resonance Raman spectra reveals two distinguishable ν_{Fe-C} bands ($\sim$490 and $\sim$510 cm^{-1}) at both pH values. These bands display the expected ^{13}CO isotope dependence and correspond to the $\nu_{C=O}$ bands at $\sim$1969 and $\sim$1950 cm^{-1}. Unlike infrared bands, the relative intensities of the resonance bands are not a direct reflection of the relative populations of configurations. Since the electronic structure of the Fe–C–O unit is clearly different for the two observable HbCO configurations, the coupling of the Fe–C vibration to the heme Soret transition and hence resonance Raman cross sections can vary dramatically as a function of heme–CO configuration. A careful study of ν_{Fe-C} excitation profiles of MbCO by Champion et al. (1989) revealed that the coupling strength of the A_0 state (ν_{Fe-C} = 491 cm^{-1}) was larger than that of the A_1 state (ν_{Fe-C} = 508 cm^{-1}). For HbCO, the ratio of the areas of the $\sim$490- and $\sim$507-cm^{-1} ν_{Fe-C} bands clearly exceeds that of the $\sim$1969- and $\sim$1952-cm^{-1} $\nu_{C=O}$ bands (Table I). Thus, the relative cross section (at 413 nm) of the $\sim$490-cm^{-1} configuration is significantly larger than that of the $\sim$510-cm^{-1} configuration. This suggests that, in this species, the more weakly bound CO is more effectively coupled into the heme Soret transition.

Structural Implications of Fe–CO Vibrations. Examination of ν_{Fe-CO} and $\nu_{C=O}$ behavior can lend insight into the structural origins of the multiple equilibrium Fe–C–O configurations in HbCO. In view of the extensive π interactions within the Fe–C–O system, it is not surprising that bond strengths of these two modes are related. Indeed, an inverse correlation between ν_{Fe-CO} and $\nu_{C=O}$ exists among a wide variety of heme proteins and model complexes:

$$\nu_{Fe-CO} = 1935 - (0.73)\nu_{CO}$$

This relationship was recently examined in some detail by Li and Spiro (1988). They concluded that systems obeying this relationship do so because of π backbonding interactions between the iron and CO. Any perturbation that decreases backbonding between Fe(π) and CO(π^*) orbitals increases the bond order of the CO bond and decreases that of the Fe–C bond. Since the values, obtained in this study, for ν_{Fe-C} and $\nu_{C=O}$ for HbCO fit this relationship within the scatter observed for heme proteins [see Li and Spiro (1988)], the difference between the major and minor configurations can be attributed to Fe–CO backbonding. Thus, decreasing the pH favors a heme–CO species in which there is less Fe–CO backbonding.

Several potentially pH-sensitive phenomena might, in principle, affect this degree of backbonding, including hydrogen bonding to the CO, proximal pocket geometry changes that affect the Fe–His(F8) bond strength, and sterically induced deviations of the Fe–C–O from the preferred linear geometry perpendicular to the plane of the porphyrin. Recent investigations of site-directed mutants of Hb and Mb (Morikis et al., 1989; Lin et al., 1990) have convincingly demonstrated that distal heme pocket interactions are responsible for the distinct Fe–C and C–O modes. Specifically, the distal histidine (E7) plays a crucial role in modulating both the electronic and steric properties of the Fe–C–O unit. Champion et al. (1989) examined myoglobin mutants in which His-E7 was replaced by either Gly or Met and found that protonation of His-E7 was responsible for the pH-induced population redistribution among Fe–CO configurations. They associated the $\nu_{Fe-C} \approx 490$ cm^{-1} configuration with a more "open" heme pocket containing a protonated His-E7. Nagai et al. (1990) characterized the spectroscopic properties and ligand affinity of both His-E7 and Val-E11 mutants of HbCO. While mutations at E11 produced no effect on ligand modes, substitution of either Gly or Phe at E-7 shifted ν_{Fe-C} and $\nu_{C=O}$ to 494 and 1970 cm^{-1}, respectively. Since Phe is as large as His, but Gly is much smaller, the authors concluded that distal heme pocket polarity, rather than steric hindrance, is the primary determinant of Fe–C and C–O mode frequencies.

Our data can best be interpreted in terms of the overall model of Li and Spiro (1988) and the hypothesis that the minor configuration with $\nu_{C=O}$ at $\sim$1970 cm^{-1} and ν_{Fe-C} at $\sim$490 cm^{-1} corresponds to a distal heme pocket structure that is less sterically restrictive and/or less polar than that of the major configuration ($\sim$1950 and $\sim$510 cm^{-1}). Neither configuration appears to be very sensitive to pH variation over the 4.5–6.5 range. Both the $\sim$490- and $\sim$510-cm^{-1} bands shift to slightly lower energy but do not broaden as the pH is lowered to 4.5. The equilibrium between the two configurations does, however, shift slightly in favor of the less constrained heme pocket at lower pH.

Dynamics of the Rebound Hemes. The transient RRS data obtained in this study probe the structural dynamics associated

with ligand rebinding in hemoglobin on several different levels. Previous time-resolved resonance Raman studies of photolyzed hemoglobins have established that the relaxation of the proximal heme pocket to its equilibrium deoxy configuration occurs on 1-μs to 1-ms time scales, depending on the particular Hb species and solution conditions employed [Rousseau & Friedman, 1988; Scott and Friedman (1984) and references therein]. Under the conditions employed in this study [low pH ($\sim$6.5) in the presence of allosteric effectors], proximal heme pocket relaxation occurs with a half-life of between 10 and 100 μs. Time-resolved absorption studies by Hofrichter et al. (1983) have shown that several relaxation processes occur after dissociation of CO from Hb. In particular, relaxation I, occurring at 40–50 ns, may reflect an evolving distal pocket environment. Thus, it is apparent that the submicrosecond CO rebinding in photolyzed Hb occurs within a structurally dynamic heme pocket. The implications of these structural dynamics on the Fe–CO bonding can be monitored through heme–ligand modes evident in the time-resolved resonance Raman spectra.

Our data clearly show that the rebound heme sites assume their equilibrium disposition within 500 ns of ligand rebinding. This behavior contrasts with the much slower ($\tau_{1/2} > 1$ μs) evolution of the proximal heme pocket of transient deoxy species created by ligand photolysis. Thus, while the unrelaxed proximal geometry has a profound effect on the kinetic barrier to ligand recombination [Rousseau & Friedman (1988) and references therein], it has little or no influence on the distal geometry of the rebound complex, even on a submicrosecond time scale. It has previously been shown that ν_{Fe-C} and $\nu_{C=O}$ of equilibrium CO-bound hemoglobins are not influenced by tertiary or quaternary structural changes of the globin (Rousseau et al., 1984). The results of this study corroborate those observations and further suggest that the six-coordinate histidine–heme–CO complex becomes structurally rigid soon ($\sim$500 ns) after CO binding, thereby locking the Fe–C mode into its equilibrium characteristics regardless of the proximal heme pocket structure of the initial deoxy species. Any changes in structure or energetics accompanying CO rebinding to deoxy hemes in different stages of relaxation must be rapidly (i.e., <500 ns) accommodated by degrees of freedom not directly at the six-coordinate heme.

On even faster (100 ns) time scales, there is no convincing evidence for metastable, transient configurations. The positions and line widths of ν_{Fe-C} during rebinding are, within error, the same as those of the equilibrium species for both heme–CO configurations. It is apparent that either the geminate ligand rebinding occurs via the dominant configurations and conformations available within the equilibrium distal pocket or relaxation to the equilibrium configurations occur on time scales significantly faster than 100 ns. Thus, it is unlikely that wholesale structural perturbations occur in the distal heme pocket on time scales comparable to those observed for proximal heme pocket relaxation.

The spectroscopically distinct distal pocket configurations of MbCO are also kinetically distinct at low temperatures (Ansari et al., 1987; Chance et al., 1987). In fact, under cryogenic conditions, there is considerable variability in the recombination activation barrier between the A_3 substate and the dominant configuration (A_1). Our data reveal small but significant differences in rebinding rates at room temperature between the two configurations seen in the time-resolved RRS spectra of HbCO. It is clear that the $\sim$490-cm^{-1} configuration is present in larger proportion in the 100-ns spectra relative to the equilibrium spectra and thus rebinds more rapidly than the $\sim$505-cm^{-1} configuration. Within 500 ns of CO photolysis, however, the $\sim$490- and $\sim$505-cm^{-1} forms are present in equilibrium proportions despite the fact that no significant additional CO rebinding (as reflected in the behavior of ν_4) occurs between the 100- and 500-ns time points. It follows that some conversion from the $\sim$490- to the $\sim$505-cm^{-1} configuration must occur during that interval.

This observation is consistent with the results of previous studies of MbCO by Frauenfelder et al. (1987). They found that the four MbCO substates readily interconvert at room temperature and low pH conditions but that this process could be suppressed by lowering the temperature or embedding the protein in a solid matrix. At low temperature (<180 K), the rebinding of photolyzed CO was found to proceed without interconversion among substates. Our data clearly suggest that, in HbCO at room temperature, interconversion between configurations occurs at rates competitive with CO rebinding. Moreover, the interconversion dynamics are apparently sensitive to solution conditions. The increase in the relative intensity of the $\sim$490-cm^{-1} band at 100 ns is larger for the pH 4.5 sample than for the pH 6.5 + IHP sample. Thus, either the difference in the time scales for CO rebinding to the two dominant configurations is smaller at pH 6.5 + IHP than at pH 4.5 or the interconversion rate is faster.

CONCLUSIONS

The data presented in this study indicate the following. (1) Heme sites of HbCO assume their equilibrium geometries within 500 ns of ligand rebinding. This is much faster than the relaxation of the proximal hemepocket to its equilibrium position subsequent to ligand photolysis. (2) Ligand rebinding (on a 100-ns time scale) occurs via the heme–CO configurations observed at equilibrium. (3) The rebinding rate for the $\sim$490-cm^{-1} configuration appears to be slightly faster than that of the major configuration. (4) Under room-temperature, low-pH conditions, interconversion from the $\sim$490- to the $\sim$505-cm^{-1} configuration occurs on a submicrosecond time scale. It should be noted that these conclusions apply only to molecules undergoing geminate recombination where the ligand presumably has not exited the distal pocket.

SUPPLEMENTARY MATERIAL AVAILABLE

One figure, showing deoxyhemoglobin at pH 4.5 examined by probe-only and Δt = 35 ns pump/probe methods (1 page). Ordering information is given on any current masthead page.

REFERENCES

Ansari, A., et al. (1987) *Biophys. Chem. 26*, 337–355.
Antonini, E., & Brunori, M. (1971) in *Hemoglobin and Myoglobin and Their Reactions with Ligands*, pp 1–3, North-Holland, Amsterdam.
Carson, S. D., Wells, C. A., Findsen, E. W., Friedman, J. M., & Ondrias, M. R. (1987) *J. Biol. Chem. 262*, 3044–3051.
Chance, M. R., Campbell, B. F., Hoover, R., & Friedman, J. M. (1987) *J. Biol. Chem. 262*, 6959–6961.
Dasgupta S., Spiro, T. G., Johnson, C. K., Dalickas, G. A., & Hochstrasser, R. M. (1985) *Biochemistry 24*, 5295–5297.
Debrunner, P. G., & Frauenfelder, H. (1982) *Annu. Rev. Phys. Chem. 33*, 283–299.
Findsen, E. W., Friedman, J. M., Ondrias, M. R., & Simon, S. R. (1985a) *Science 229*, 661–665.
Findsen, E. W., Scott, T. W., Chance, M. R., Friedman, J. M., & Ondrias, M. R., (1985b) *J. Am. Chem. Soc. 107*, 3355–3357.
Findsen, E. W., Simon, S. R., & Ondrias, M. R., (1986) *Biochemistry 25*, 7912.

Findsen, E. W., Friedman, J. M., & Ondrias, M. R., (1988) *Biochemistry 27*, 8719–8724.
Friedman, J. M. (1984) *Science 228*, 1273–1280.
Friedman, J. M., & Lyons, K. B. (1980) *Nature 284*, 570–572.
Friedman, J. M., Rousseau, D. L., & Ondrias, M. R. (1982a) *Annu. Rev. Phys. Chem. 33*, 471–491.
Friedman, J. M., Rousseau, D. L., Ondrias, M. R., & Stepnoski, R. A. (1982b) *Science 218*, 1244–1246.
Hofrichter, J., Sommer, J. H., Henry, E. R., & Eaton, W. A. (1983) *Proc. Natl. Acad. Sci. U.S.A. 80*, 2235–2239.
Karplus, M., & McCammon, A. (1983) *Annu. Rev. Biochem. 53*, 263–300.
Kerr, E. A., & Yu, N.-T. (1988) in *Biological Applications of Raman Scattering* (Spiro, T. G., Ed.) Vol. III, Wiley, New York.
Li, X.-Y., & Spiro, T. G. (1988) *J. Am. Chem. Soc. 111*, 6024–6033.
Lin, S.-H., Yu, N.-T., Tame, J., Shih, D., Renaud, J.-P., Pagnier, J., & Nagai, K. (1990) *Biochemistry 29*, 5562–5566.
Makinen, M. W., Hutchens, R. A., & Caughey, W. S. (1979) *Proc. Natl. Acad. Sci. U.S.A. 76*, 6042–6046.
Morikis, D., Champion, P. M., Springer, B. A., & Sligar, S. G. (1989) *Biochemistry 28*, 4791–4800.
Ondrias, M. R., Friedman, J. M., & Rousseau, D. L. (1983) *Science 220*, 615–619.
Potter, W. T., Hazzard, J. H., Choc, M. G., Tucker, M. P., & Caughey, W. S. (1990) *Biochemistry 29*, 6283–6295.
Rousseau, D. L., & Ondrias, M. R. (1983) *Annu. Rev. Biophys. Bioeng. 12*, 357–380.
Rousseau, D. L., & Friedman, J. M. (1988) *Biological Applications of Raman Scattering* (Spiro, T. G., Ed.) Vol. III, pp 135–213, Wiley, New York.
Rousseau, D. L., Tan, S. L., Ondrias, M. R., Ogawa, S., & Noble, R. W. (1984) *Biochemistry 23*, 2857–2865.
Scott, T. W., & Friedman, J. M. (1984) *J. Am. Chem. Soc. 106*, 5677–5687.
Shimada, H., & Caughey, W. S. (1982) *J. Biol. Chem. 257*, 11893–11900.
Spiro, T. G. (1983) in *Iron Porphyrins* (Lever, A. B. P., & Gray, H. B., Eds.) Vol. II, pp 89–139, Addison-Wesley, Reading, MA.
Stein, P., Terner, J., & Spiro, T. G. (1982) *J. Phys. Chem. 86*, 168–172.
Terner, J., Strong, J. D., Spiro, T. G., Nagumo, M., Nicol, M. S., & El-Sayed, M. A. (1981) *Proc. Natl. Acad. Sci. U.S.A. 78*, 1313–1317.